Stokes Modes in Taylor-Couette Geometry

Thomas Gebhardt and Siegfried Grossmann
Fachbereich Physik, Philipps-Universität Marburg, Marburg, FRG

Z. Naturforsch. **46a**, 669–676 (1991); received May 24, 1991

The eigenvalue problem of the Stokes operator is solved for an incompressible fluid contained between two coaxial cylinders of infinite height. Flow field patterns and spectra of the eigenmodes ("Stokes modes") are offered. Furthermore, in finite dimensional subspaces generated by these Stokes modes, the eigenproblem for the Navier-Stokes operator linearized about the laminar Taylor-Couette flow is studied. Although the spectrum's qualitative features are still correct, we quantitatively obtain wrong results. We trace this back to a Gibbs like phenomenon of higher order derivatives of the flow field as probable source, since the Stokes modes do not reflect the discontinuity arising from different velocities at both cylinders.

1. Introduction

One of the basic techniques in solving fluid dynamical problems is mode decomposition: one approximates the partial differential equation for the time evolution of the velocity field (i.e., the Navier-Stokes equation) by a finite set of ordinary differential equations. Especially in the context of investigating hydrodynamic instabilities this method – often denoted as Galerkin method – seems pretty useful. In this paper, however, we demonstrate for the well known Taylor instability [1], that an evident choice of the set of the expansion modes can lead to erroneous results.

The instabilities of fluid motion between rotating coaxial cylinders ("Taylor-Couette system") have been investigated since about one hundred years. Chandrasekhar [2] has established a simple but powerful Galerkin-type method to calculate the onset of linear instability caused by the rotation of the inner cylinder. Up till now his method has been used in a variety of problems in hydrodynamics [3]. Its basic idea is to eliminate analytically as many components of the Navier-Stokes equation as possible and expand the remaining fields into a suitable set of modes. The field components that are eliminated analytically are selected by convenience and therefore somewhat arbitrarily. But one can also expand the stream function into a series of modes [4] or decompose the whole velocity field into vector modes [5], thereby treating all velocity components in the same manner. This latter method is not restricted to linear stability theory but can be extended to deal with nonlinear mode interaction in a straight forward way.

The geometry of the system under consideration is shown in Figure 1.1. We restrict ourselves to cylinders of large aspect ratio Γ, i.e., effects generated by the bottom or top plates are neglected.

The motion of an incompressible fluid is governed by the Navier-Stokes equation (NSE):

$$\partial_t \boldsymbol{U}(\boldsymbol{x}, t) = -(\boldsymbol{U}(\boldsymbol{x}, t) \cdot \nabla)\, \boldsymbol{U}(\boldsymbol{x}, t) + \nu \Delta \boldsymbol{U}(\boldsymbol{x}, t) - \nabla P(\boldsymbol{x}, t), \tag{1.1}$$

together with the continuity equation

$$\nabla \cdot \boldsymbol{U}(\boldsymbol{x}, t) = 0\,. \tag{1.2}$$

$\boldsymbol{U}(\boldsymbol{x}, t)$ stands for the velocity field, $P(\boldsymbol{x}, t)$ denotes the pressure per unit mass and ν is the kinematic viscosity of the fluid.

Equations (1.1) and (1.2) admit the laminar solution

$$\boldsymbol{U}_0(\boldsymbol{x}, t) = U_0(r)\, \boldsymbol{e}_\varphi\,, \tag{1.3}$$

$$P_0(r, t) = \int_{r_1}^{r} \frac{U_0^2(\varrho)}{\varrho}\, \mathrm{d}\varrho + P_0(r_1, t)\,, \tag{1.4}$$

with

$$U_0(r) = A r + \frac{B}{r}\,. \tag{1.5}$$

The no slip condition at the cylinder walls determines the constants A and B for the laminar Couette flow in terms of the Reynolds numbers $\mathscr{R}_\alpha$ and the radius ratio η:

$$A = \frac{\mathscr{R}_2 - \eta \mathscr{R}_1}{1+\eta}\, \frac{\nu}{d^2}\,, \tag{1.6}$$

$$B = \frac{\eta(\mathscr{R}_1 - \eta \mathscr{R}_2)}{(1-\eta)(1-\eta^2)}\, \nu\,. \tag{1.7}$$

Reprint requests to Prof. Dr. S. Grossmann, Fachbereich Physik, Universität Marburg, Renthof 6, W-3550 Marburg, FRG.

0932-0784 / 91 / 0800-0669 $ 01.30/0. – Please order a reprint rather than making your own copy.

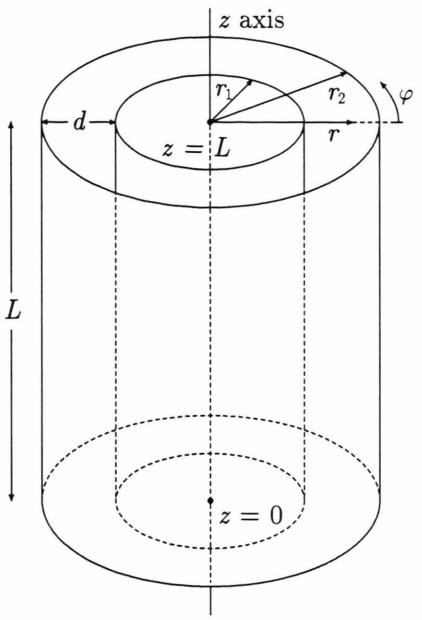

Fig. 1.1. Geometry and coordinates $r \in [r_1, r_2]$, $\varphi \in [0, 2\pi)$, $z \in [0, L]$ of the Taylor-Couette system. The relevant parameters are the radius ratio $\eta = r_1/r_2$, the aspect ratio $\Gamma = L/d$, the inner (ω_1) and outer (ω_2) cylinder's angular velocities, and the inner and outer Reynolds numbers $\mathscr{R}_{1,2}$, with $\mathscr{R}_\alpha = r_\alpha \omega_\alpha d/\nu$, $\alpha = 1, 2$.

All numerical values that are given in the next sections will refer to multiples of the slit width d as the length scale and to the viscous diffusion time d^2/ν as the time scale. ν/d will serve to measure velocities and ν^2/d^2 does it for the kinematic pressure.

2. Mode Decomposition

In order to transform the NSE (1.1) into a set of ordinary differential equations, we first subdivide the velocity field $\boldsymbol{U}(\boldsymbol{x}, t)$ into the basic Couette flow $\boldsymbol{U}_0(x)$ and a perturbation $\boldsymbol{u}(\boldsymbol{x}, t)$, which is not necessarily small. The same we do for the pressure $P(\boldsymbol{x}, t)$.

$$\boldsymbol{U}(\boldsymbol{x}, t) = \boldsymbol{U}_0(\boldsymbol{x}) + \boldsymbol{u}(\boldsymbol{x}, t), \tag{2.1}$$

$$P(\boldsymbol{x}, t) = P_0(\boldsymbol{x}) + p(\boldsymbol{x}, t). \tag{2.2}$$

Next, the deviation of the velocity from the laminar profile is decomposed into a set of modes:

$$\boldsymbol{u}(\boldsymbol{x}, t) = \sum_j a_j(t)\, \boldsymbol{u}_j(\boldsymbol{x}). \tag{2.3}$$

The index j here labels the modes (not the components of the velocity).

The NSE and the continuity equation now read

$$\sum_j \dot{a}_j(t)\, \boldsymbol{u}_j(\boldsymbol{x}) = -\sum_j a_j(\boldsymbol{U}_0 \cdot \nabla)\, \boldsymbol{u}_j - \sum_j a_j(\boldsymbol{u}_j \cdot \nabla)\, \boldsymbol{U}_0 - \sum_{j,k} a_j a_k(\boldsymbol{u}_j \cdot \nabla)\, \boldsymbol{u}_k + \nu \sum_j a_j \Delta \boldsymbol{u}_j - \nabla p, \tag{2.4}$$

$$\sum_j a_j(\nabla \cdot \boldsymbol{u}_j) = 0. \tag{2.5}$$

In this dimensionless form of the NSE it is $\nu = 1$, but we keep ν in (2.4) as a marker.

Three restrictions on the set of modes $\{\boldsymbol{u}_j(\boldsymbol{x})\}$ make these equations more convenient:

- First we demand each mode $\boldsymbol{u}_j(\boldsymbol{x})$ to satisfy the boundary condition $\boldsymbol{u}_j(r)|_{r=r_1, r_2} = 0$.
- Second we require $\nabla \cdot \boldsymbol{u}_j = 0$ for all modes $\boldsymbol{u}_j$.
- Third the number of modes N is taken as finite.

Thus the no slip condition at the cylinder walls and the continuity equation are trivially fulfilled by the ansatz (2.3).

To eliminate the pressure we take the curl on both sides of (2.4), using the abbreviation $\vec{\omega}_j := \operatorname{rot} \boldsymbol{u}_j$:

$$\sum_j \vec{\omega}_j \dot{a}_j = \sum_j a_j \operatorname{rot}(\boldsymbol{U}_0 \times \vec{\omega}_j + \boldsymbol{u}_j \times \operatorname{rot} \boldsymbol{U}_0) + \nu \sum_j a_j \Delta \vec{\omega}_j + \sum_{j,k} a_j a_k \operatorname{rot}(\boldsymbol{u}_j \times \vec{\omega}_k). \tag{2.6}$$

We define the scalar product of two vector fields $\langle \boldsymbol{u} | \boldsymbol{v} \rangle$ as the integral $\int \boldsymbol{u}^* \cdot \boldsymbol{v}\, \mathrm{d}V/V$ over the space between the two cylinders and multiply (2.6) by $\vec{\omega}_i$. In an obvious notation (e.g. $W_{ij} := \langle \vec{\omega}_i | \vec{\omega}_j \rangle$) one gets

$$\sum_j W_{ij} \dot{a}_j = \sum_j L_{ij} a_j + \nu \sum_j D_{ij} a_j + \sum_{j,k} N_{ijk} a_j a_k. \tag{2.7}$$

This is a set of ordinary differential equations for the expansion coefficients $a_j(t)$, in principle infinite, practically approximated by a finite set. The first term on the r.h.s. of (2.7) represents the stirring influence of the basic profile $\boldsymbol{U}_0$, the second and damping term is due to viscosity and the last one comes from the NSE nonlinearity and yields a nonlinear mode interaction.

3. Stokes Modes

3.1. Calculation of the Stokes Modes

Of course, requiring vanishing divergence and no slip boundary conditions does not determine the set of modes uniquely. So one still has some freedom to choose a convenient or the most appropriate set.

Since the eigenvalue problem of the Stokes operator (i.e., the linearized Navier-Stokes operator with vanish-

ing $\boldsymbol{U}_0$) can be solved almost analytically, it seems evident to use its eigenmodes (hereafter called "Stokes modes") as the basis for our expansion. This was also extensively done e.g. in [5]. So we first have to investigate the solutions of the "Stokes equations"

$$\nu \Delta \boldsymbol{u} - \nabla p = -\alpha^2 \boldsymbol{u}\,, \tag{3.1}$$

$$\nabla \cdot \boldsymbol{u} = 0\,, \tag{3.2}$$

with $\boldsymbol{u}(r)|_{r=r_1,r_2} = 0$ and periodic boundary conditions at $z = 0, L$.

When solving the eigenvalue problem (3.1), (3.2) one is faced with the fact that the Laplacean – when expressed in cylindrical coordinates – mixes the three components of the vector $\boldsymbol{u}$. In order to separate this vector eigenvalue problem we make the ansatz [5]

$$\boldsymbol{u} = \mathrm{rot}\,(a\,\boldsymbol{e}_z) + \mathrm{rot}\,\mathrm{rot}\,(b\,\boldsymbol{e}_z) + \nabla c \tag{3.3}$$

with scalar functions a, b, c. The pressure is given then by

$$p = \frac{\alpha^2}{\nu}\, c + p_0\,. \tag{3.4}$$

Every solution of (3.1), (3.2) in Taylor-Couette geometry can be expressed in the form (3.3), cf. [6]. Equation (3.1) separates into three equations:

$$\nu \Delta a = -\alpha^2 a\,, \tag{3.5}$$

$$\nu \Delta b = -\alpha^2 b\,, \tag{3.6}$$

$$\Delta c = 0\,, \tag{3.7}$$

which can easily be solved by Bessel functions (put now $\nu = 1$):

$$a = (A_1 J_m(sr) + A_2 Y_m(sr))\, e^{i(m\varphi + \beta z)}\,, \tag{3.8}$$

$$b = (B_1 J_m(sr) + B_2 Y_m(sr))\, e^{i(m\varphi + \beta z)}\,, \tag{3.9}$$

$$c = \begin{cases} (C_1 I_m(\beta r) + C_2 K_m(\beta r))\, e^{i(m\varphi + \beta z)} & \text{if } \beta \neq 0, \\ (C_1 r^m + C_2 r^{-m})\, e^{im\varphi} & \text{if } \beta = 0 \end{cases} \tag{3.10}$$

with integer m, constant coefficients $A_1, \ldots, C_2$, and $s := \sqrt{\alpha^2 - \beta^2}$. The axial wavenumber β in principle is restricted to values of integer multiples of $2\pi/L$ but is treated as a continuous variable since the aspect ratio $\Gamma = L/d$ is large and has been left unspecified. The boundary condition $\boldsymbol{u}(r)|_{r=r_1,r_2} = 0$ implies a system of linear homogeneous equations for the coefficients $A_1, \ldots, C_2$ that has nontrivial solutions only for certain discrete values of α^2. One can normalize the resulting Stokes modes requiring $\langle \boldsymbol{u}_j | \boldsymbol{u}_j \rangle = 1$. Since the eigenvalue problem (3.1), (3.2) is Hermitean, eigen-

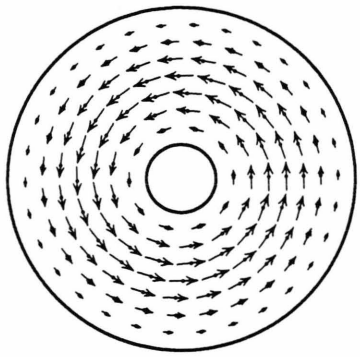

Fig. 3.1. Cross section of flow pattern for the first (i.e., no inner r-node) Stokes mode of class 1; $\boldsymbol{u} \cdot \boldsymbol{e}_z$ is zero, $\eta = 0.2$, $\alpha^2 = 11.48$. Modes of class 3 (not displayed) look similar but are sinusoidally modulated in amplitude along the cylinder axis.

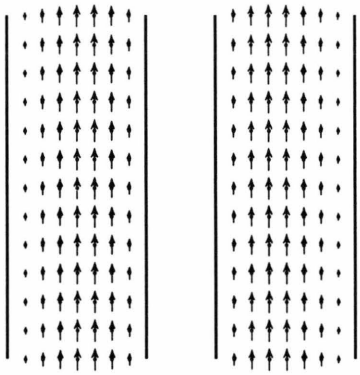

Fig. 3.2. Cross section along the cylinder axis. The plot shows the first (no r-node) Stokes mode of class 2; $\eta = 0.2$, $\alpha^2 = 9.32$. Modes of class 4 (not displayed) look similar but are sinusoidally modulated in amplitude in azimuthal direction.

Table 3.1. Classification of Stokes modes. $m = 0, \pm 1, \ldots$ is the azimuthal wave number, $\beta \in R$ is the axial wavenumber and p denotes the pressure of the Stokes mode flow field.

Class	m	β	Flow characteristics	p field
1	0	0	Flow only in azimuthal direction	0
2	0	0	Flow only parallel to the cylinder axis	0
3	0	$\neq 0$	Flow only in azimuthal direction	0
4	$\neq 0$	0	Flow only parallel to the cylinder axis	0
5	$\neq 0$	0	Flow perpendicular to $\boldsymbol{e}_z$	$\neq 0$
6	0	$\neq 0$	Vortices around the cylinder axis	$\neq 0$
7	$\neq 0$	$\neq 0$	"Spiral staircase" flow	$\neq 0$
8	$\neq 0$	$\neq 0$	Twisted vortices around the axis	$\neq 0$

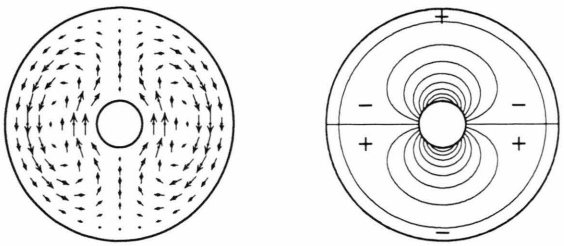

Fig. 3.3. First (lowest inner radial node number) Stokes mode of class 5, $m=1$, $\eta=0.2$, $\alpha^2=37.80$. The contour lines of the pressure are equally spaced with an increment of 2 in terms of ν^2/d^2. For water ($\varrho_0 \cong 10^3$ kg m^{-3} and $\nu \cong 10^{-6}$ m^2 s^{-1}) in a $d=10^{-2}$ m slit this corresponds to a physical pressure increment of 2 in multiples of 10^{-5} Nm^{-2} or 10^{-10} atm. The normalisation condition $\langle \boldsymbol{u}_j \mid \boldsymbol{u}_j \rangle = 1$ fixes $|\boldsymbol{u}|$ to an order of ν/d, which is 10^{-4} m s^{-1} in our example.

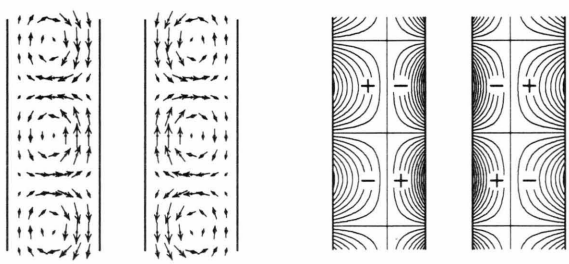

Fig. 3.4. Cross section of first (lowest inner radial node number) mode of class 6 parallel to the cylinder axis, $\beta=\pi$, $\eta=0.2$, $\alpha^2=38.07$. Spacing of the contour lines of the pressure is 50.

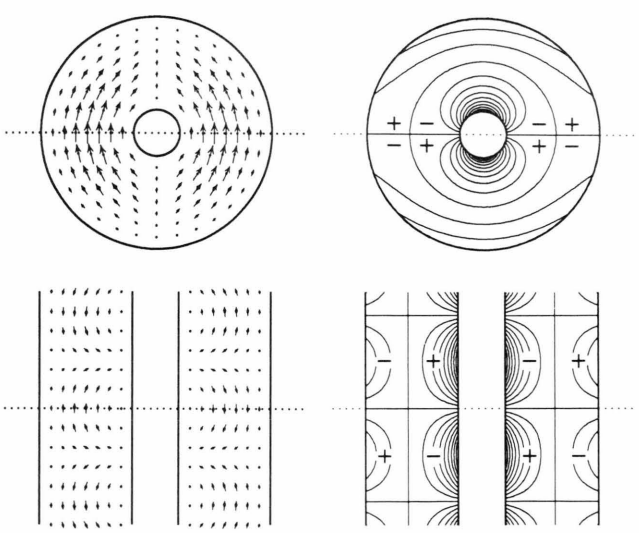

Fig. 3.5. First (no inner radial node) Stokes mode of class 7, $m=1$, $\beta=\pi$, $\eta=0.2$, $\alpha^2=22.12$. Flow is three dimensional, so only the projections of the velocities are plotted. Sections perpendicular and parallel to the axis, the dotted lines should be identified. Spacing of the contour lines of the pressure is 20.

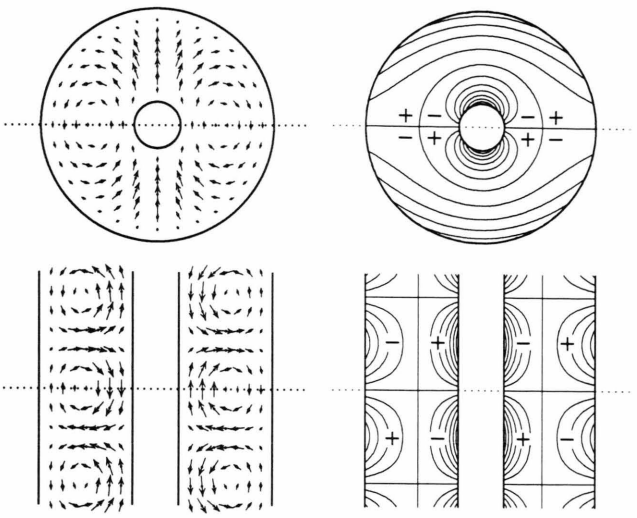

Fig. 3.6. First Stokes mode of class 8, $m=1$, $\beta=\pi$, $\eta=0.2$, $\alpha^2=39.23$. The arrows indicate the projections of the velocity, spacing of the contour lines of the pressure is 100.

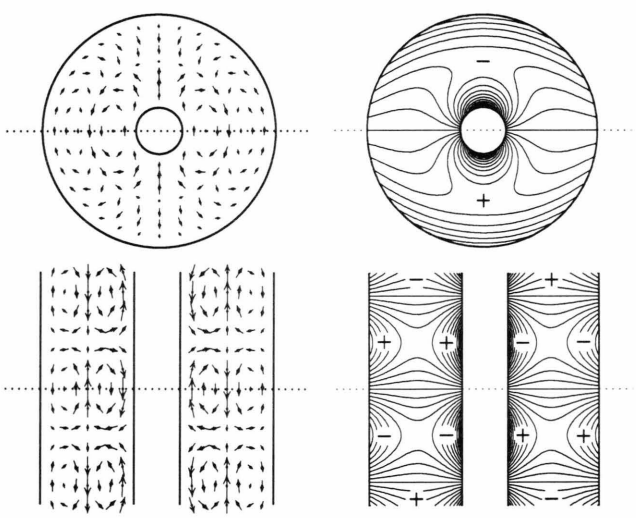

Fig. 3.7. Second Stokes mode of class 8. m, β, and η are the same as in Figure 3.6. The eigenvalue α^2 is 87.11, the spacing of the contour lines of the pressure is 200. The pressure is positive where the fluid approaches the wall and negative where it leaves the wall.

functions with different eigenvalues α_j^2 are orthogonal. Furthermore, the spectrum of the Stokes operator is negative definite, i.e., α^2 is real and positive.

3.2. Stokes Modes' Classification and Examples

One can classify the Stokes modes of the Taylor-Couette system into eight classes of qualitatively dis-

tinct flow patterns. Table 3.1 gives a list of them, whose discussion follows.

Each class consists of hierarchies i.e., subclasses of modes with fixed m and β, but with an arbitrary number of nodes in radial direction apart from those at r_1 and r_2. Examples are presented in Figs. 3.1–3.7. They show the projections of the flow patterns and contour lines of the pressure on cross sections parallel and perpendicular to the cylinder axis. The radius ratio η is 0.2. If the fluid flow near a wall approaches this wall, the pressure becomes positive; leaving the wall it gets negative.

By the choice of periodic boundary conditions in z-direction one identifies the top and the bottom of the cylinder. So, from a topological viewpoint, the flow domain is a toroidal shell, for which φ and z are the angle variables. But the metric distinguishes between φ and z: space is curved along $\boldsymbol{e}_\varphi$ but flat along $\boldsymbol{e}_z$.

By interchanging the variables φ and z in the Stokes mode of Fig. 3.1, one gets a velocity field that is topologically equivalent to Fig. 3.2, and vice versa. In this sense classes 1 and 2, 3 and 4, 5 and 6 are dual.

3.3. The Eigenvalue Spectrum of the Stokes Modes

One can compare the eigenvalues of (3.1), (3.2) with the spectrum of the Laplacean in flat space

$$\nu \Delta \boldsymbol{v} = -\alpha^2 \boldsymbol{v} \tag{3.11}$$

in the domain

$$(x, y, z) \in [0, 1] \times [0, 2\pi r_m] \times [0, L]; \quad r_m := (r_1 + r_2)/2,$$

which has the solution (again putting $\nu = 1$)

$$\begin{pmatrix} x \\ y \\ z \end{pmatrix} = \begin{pmatrix} C_x \\ C_y \\ C_z \end{pmatrix} \cdot \sin(n\pi x)\, e^{i(my/r_m + \beta z)}, \tag{3.12}$$

where

$$\alpha^2 = (\pi n)^2 + (m/r_m)^2 + \beta^2. \tag{3.13}$$

On comparing the flat space solutions with the solutions of the Stokes equations (3.1), (3.2) one observes:

- The continuity equation (3.2) excludes those solutions of the form (3.12) that have nonzero divergence. On the other hand, the pressure term in (3.1) admits a new type of solutions that form rolls like those appearing in the Rayleigh-Benard system.
- The curvature (only slightly) modifies the eigenvalues and the eigenvectors but does not change them qualitatively. (As the only exception to this rule the curvature gives rise to a nonzero pressure field of the modes of class 7 although they are essentially of type (3.12).)

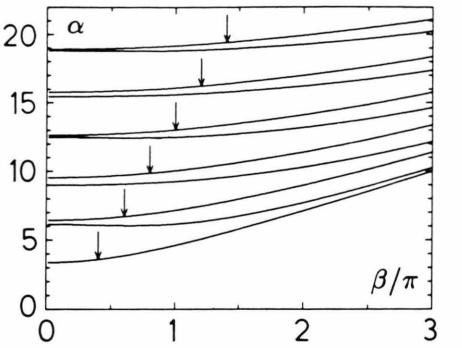

Fig. 3.8. Part of the eigenvalue spectrum of the Stokes equations (3.1), (3.2) as it changes with the wave number β, fixed $m=1$, $\eta=0.2$. The eigenvalues marked by an arrow coincide – within an error that is smaller than the line width – with the curves $\alpha = \sqrt{(\pi n)^2 + (m/r_m)^2 + \beta^2}$, $n = 1, 2, \ldots, 6$ (cf. (3.13)).

Figure 3.8 shows the least stable eigenvalues of (3.1) and (3.2) for $m=1$, $\eta=0.2$. The lines indicated by an arrow belong to the modes of class 7. They can also be regarded as originating from (3.13), since their deviation from the corresponding solutions of the Stokes equations (3.1), (3.2) is smaller than the line width. The other eigenvalues are of class 8.

In a flat geometry (e.g. in the Rayleigh-Benard system) there would be no distinction between modes of class 3, 4, and 7 or modes of class 5, 6, and 8, respectively. But in our curved geometry this degeneracy is removed since, for example, the rolls are either parallel to $\boldsymbol{e}_z$ (class 5) or parallel to $\boldsymbol{e}_\varphi$ (class 6) or oblique (class 8).

Quite generally the Stokes spectrum follows quite closely the spectrum of the Laplacean except for the just mentioned proviso.

4. Linear Stability of the Laminar Taylor-Couette Flow

4.1. Critical Reynolds Number

To test how suitable it is to use the Stokes modes in the expansion (2.3) we tried to reproduce the well known linear instability for axisymmetric disturbances of the Couette flow induced by a resting outer and a rotating inner cylinder. Therefore we calculated the matrix elements W_{ij}, L_{ij}, and D_{ij} of (2.7) to study the eigenvalue problem

$$\lambda \sum_j W_{ij}\, a_j = \sum_j L_{ij}\, a_j + \nu \sum_j D_{ij}\, a_j. \tag{4.1}$$

Integrating by parts and using (3.1) one gets

$$W_{ij} = \frac{1}{\nu} \alpha_i^2 \, \delta_{ij} \,, \tag{4.2}$$

$$D_{ij} = -\frac{1}{\nu^2} \alpha_i^4 \, \delta_{ij} \,. \tag{4.3}$$

Because the Stokes modes $\boldsymbol{u}_j$ vanish at the cylinder walls there are no surface terms from integrating by parts. One can calculate L_{ij} directly in the form derived from (2.6), or one may also integrate by parts, obtaining

$$L_{ij} = -\langle \Delta \boldsymbol{u}_i \mid \boldsymbol{U}_0 \times \vec{\omega}_j + \boldsymbol{u}_j \times (\mathrm{rot}\, \boldsymbol{U}_0) \rangle \,. \tag{4.4}$$

(Although $\boldsymbol{U}_0$ does not vanish at the cylinder walls, the boundary terms again vanish since only $\boldsymbol{U}_0 \cdot \boldsymbol{e}_r$ appears.) Both methods lead to the same results.

The peculiarity of the eigenvalue problem (4.1) is that it is not Hermitean. Nevertheless, for $m=0$ the spectrum can be shown to be invariant under complex conjugation. Matrix elements of L_{ij} for different values of m or β vanish because of the orthogonality of the exponentials in (3.8)–(3.10). Therefore (4.1) has block diagonal form. We took 10 ... 50 modes, labeled by their radial node number, per block. The solution of (4.1) was carried out by standard eigenvalue solvers of the IMSL-library. The eigenvalues converged very well with increasing numbers of modes; 15 modes were enough to obtain an accuracy of 10^{-4}.

The critical inner Reynolds numbers were found to be qualitatively right but shifted from the correct values (cf. [1–3]) by an amount of 10% to 30%. Figures 4.1 and 4.2 display this. Solid lines show the actual onset of linear instability (see e.g. [3, 7, 8]), dashed lines give the results of the diagonalisation with $m=0$ Stokes modes. The dependence of the critical Reynolds number on η when rotating the inner cylinder and keeping the outer one fixed is plotted in Figure 4.1. The dots are from [8], the connecting line results from shooting methods as given in [9]. Figure 4.2 shows the onset of instability of axisymmetric modes in the system of independently rotating cylinders of radius ratio $\eta=0.9$. Heavy lines and thin lines belong to the critical inner Reynolds numbers $\mathscr{R}_{1,\mathrm{cr}}$ and to the critical wavenumbers β_{cr}, respectively.

4.2. A Gibbs Phenomenon

Why does the Stokes mode expansion give systematically quantitatively wrong results? To answer this question, we take the correct eigenfunction $\boldsymbol{u}_{\mathrm{cr}}(\boldsymbol{x})$ at instability threshold $\lambda=0$ and expand it into a series of Stokes modes:

$$\boldsymbol{u}_{\mathrm{cr}}(\boldsymbol{x}) = \begin{pmatrix} u_{\mathrm{cr},r}(r) \\ u_{\mathrm{cr},\varphi}(r) \\ i\, u_{\mathrm{cr},z}(r) \end{pmatrix} e^{i\beta z} \approx \sum_{j=1}^{N} \langle \boldsymbol{u}_j \mid \boldsymbol{u}_{\mathrm{cr}} \rangle \, \boldsymbol{u}_j =: \boldsymbol{u}_{\mathrm{cr}}^{(N)} \,. \tag{4.5}$$

Again, $\boldsymbol{u}_{\mathrm{cr}}$ is obtained by shooting methods [9]. The approximation in the $\mathscr{L}_2$ sense is already good (up to 10^{-4}) for $N=10$. Figure 4.3 shows the three components of $\boldsymbol{u}_{\mathrm{cr}}$, the deviation $\boldsymbol{u}_{\mathrm{cr}}^{(50)} - \boldsymbol{u}_{\mathrm{cr}}$ is plotted in Figure 4.4. The oscillations of $\boldsymbol{u}_{\mathrm{cr},z}^{(N)} - \boldsymbol{u}_{\mathrm{cr},z}$ at the boundaries are obvious but small in amplitude. (Note the different scales of Fig. 4.3 and Figure 4.4). The amplitude of this oscillation numerically proved to decrease $\sim 1/N^2$. But the situation becomes worse for $\vec{\omega}_{\mathrm{cr}}$ (:= rot $\boldsymbol{u}_{\mathrm{cr}}$) or even $\Delta \boldsymbol{u}_{\mathrm{cr}}$. $\Delta \boldsymbol{u}_{\mathrm{cr}}$ and $\Delta(\boldsymbol{u}_{\mathrm{cr}}^{(50)})$ are plotted in Figs. 4.5 and 4.6. Here the deviations become visible on a "macroscopic" scale. The continuity equation requires $(\mathrm{d}/\mathrm{d}r + 1/r)\, u_{\mathrm{cr},r} = \beta\, u_{\mathrm{cr},z}$, so $u_{\mathrm{cr},z}$ is something like the derivative of $u_{\mathrm{cr},r}$. Hence oscillations are most visible or even dramatic for the z-components of $\boldsymbol{u}_{\mathrm{cr}}^{(N)}$ or $\Delta(\boldsymbol{u}_{\mathrm{cr}}^{(N)})$. The oscillation amplitudes of $\Delta(\vec{\omega}_{\mathrm{cr}}^{(N)})$ turn out not to decrease but even to diverge with increasing N.

Now, the L_{ij} and D_{ij} matrix elements in the eigenvalue equation (4.1) in the N-dimensional Stokes subspace contain up to three or four derivatives of the velocity components. The just obtained artificial oscillations of the derivatives plausibly increase the influence of viscosity in (4.1), which we think explains why the range of stability of the laminar flow is systematically extended in the Stokes mode analysis of the Taylor-Couette eigenvalue problem.

The oscillations observed remind one of the Gibbs phenomenon found when Fourier analysing a discontinuous function. What is discontinuous here? We think that it is the different angular velocity $\omega_1 \neq \omega_2$ of the inner cylinder compared to the outer one which is not yet present in the basis $\{\boldsymbol{u}_j\}$ of Stokes modes. Neither the Stokes equations (3.1), (3.2) nor their boundary condition $\boldsymbol{u}=0$ take notice of $\omega_1 \neq \omega_2$.

4.3. Adding "Handmade" Modes

In order to cure the Gibbs phenomenon for the higher derivatives of the flow field, we tried to add a few additional modes that were constructed with the intention to provide the system (4.1) with the possibility to compensate different boundary values for the

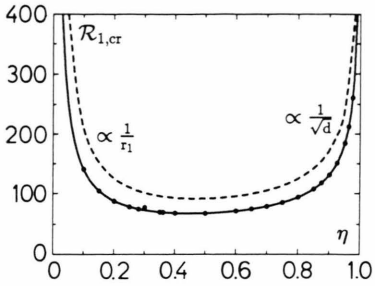

Fig. 4.1. The onset of linear instability of laminar Taylor-Couette flow with rotating inner cylinder. It is $m=0$. The dots [8] and the connecting line [9] show the correct $\mathcal{R}_{1,cr}$ as a function of radius ratio η. The dashed line gives the results of diagonalisation of (4.1) in a basis of 25 Stokes modes.

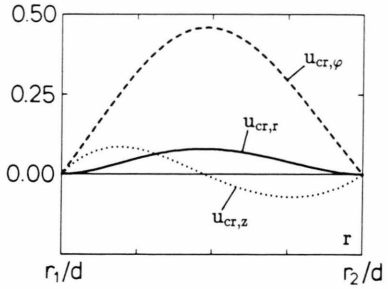

Fig. 4.3. Components of the normalized (i.e. $\langle \boldsymbol{u}_{cr} | \boldsymbol{u}_{cr} \rangle = 1$) critical mode $\boldsymbol{u}_{cr}$ at the onset of linear instability as a function of the radius r. $\mathcal{R}_{1,cr}=131.6$, $\mathcal{R}_2=0$, $\beta=3.13$, $\eta=0.9$. The velocity is given in units of ν/d.

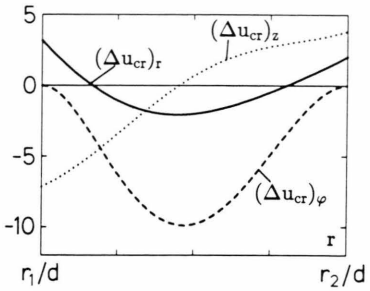

Fig. 4.5. Components of the Laplacean of the critical mode $\boldsymbol{u}_{cr}$, i.e. $(\Delta \boldsymbol{u})_{r,\varphi,z}$. Units are ν/d^3.

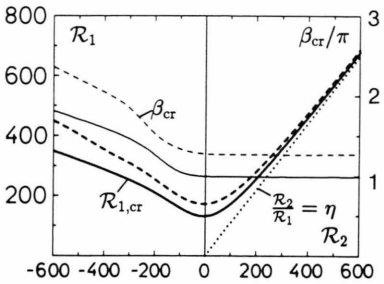

Fig. 4.2. Phase diagram for the onset of linear instability of axially symmetric ($m=0$) modes. η is choosen to be 0.9. The dotted line on the right hand side shows the Rayleigh criterion [10], which indicates linear instability for an inviscid fluid. Full and dotted lines show exact values and the results of the Stokes mode diagonalisation, respectively. The heavy lines correspond to the critical inner Reynolds numbers $\mathcal{R}_{1,cr}$, thin lines indicate the critical wavenumbers β_{cr}. It is $\mathcal{R}_{1,cr}(\mathcal{R}_2=0)=131.6$ (correct) and 171.3 (Stokes mode space), resp. $\mathcal{R}_1=100$ corresponds to $\omega_1=1/9$ Hz or period $\tau_1\approx 57$ s for a Taylor system with $\eta=0.9$, $d=10^{-2}$ m filled with water, $\nu=10^{-6}\ \mathrm{m^2\,s^{-1}}$.

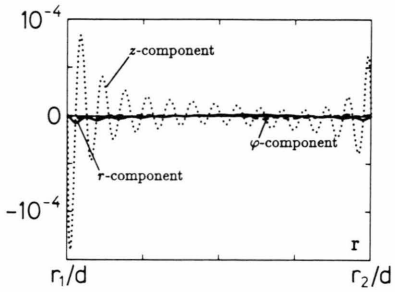

Fig. 4.4. Deviation of the Stokes mode expansion $\boldsymbol{u}_{cr}^{(50)}$ from $\boldsymbol{u}_{cr}$. The z-component strongly oscillates at the boundary. Note the smaller scale in comparison with Figure 4.3.

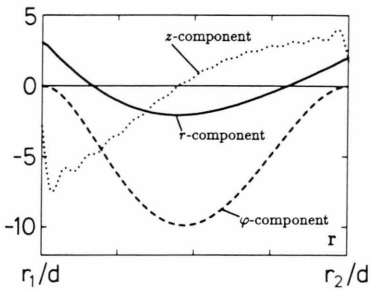

Fig. 4.6. Components of the Laplacean of the Stokes mode expansion $\boldsymbol{u}_{cr}^{(50)}$, i.e. $(\Delta \boldsymbol{u}_{cr}^{(50)})_{r,\varphi,z}$. Although the same scale as in Fig. 4.5 the Gibbs oscillations are clearly visible.

derivatives at the cylinder walls. For instance we added in (2.3), and thus in (4.1) a mode of the form

$$\boldsymbol{u}_{hm} = (f(r)\,\boldsymbol{e}_r + i g(r)\,\boldsymbol{e}_z)\, e^{i\beta z},$$

with

$$f(r)=C(r-r_1)^2(r_2-r)^3 \quad \text{and} \quad g(r)=\frac{1}{\beta}\left(\frac{\mathrm{d}}{\mathrm{d}r}+\frac{1}{r}\right) f(r).$$

Indeed, the eigenvalues were shifted towards the correct values. But for small β the modes now became too unstable. Even the matrix D_{ij} of (4.1) was no longer negative definite if we took this handmade mode plus a few Stokes modes, since $\langle \vec{\omega}_{hm} | \Delta \vec{\omega}_{hm} \rangle$ becomes positive for small values of β. This undesirably would

mean that the Taylor-Couette system with resting cylinders would be unstable to small β perturbations.

5. Conclusion

The projection of the infinite dimensional dynamics, generated by the Navier-Stokes equation, onto any finite dimensional subspace spanned by a set of modes of course always leads to approximation errors. One hopes, however, that they will become negligible if the dimension of the subspace is large enough. Our example shows that this hope can fail.

By definition the Stokes modes are the eigenmodes of the Taylor-Couette system with resting cylinders. Using these modes as an orthonormalized expansion set for the eigenmodes in the case of differently rotating cylinders fails. One can show by linear perturbation theory that the error in the eigenvalues – calculated in the context of this expansion – grows quadratically with the Reynolds number associated with that rotation. The corresponding eigenmodes exhibit a Gibbs phenomenon at the boundaries. We conjecture that similar effects will appear whenever one deals with differently moving walls in terms of Stokes modes. Chandrasekhar's method to calculate the instability [2] avoids the evaluation of higher derivatives of the flow field and therefore does not suffer from the Gibbs phenomenon that we observed. We detected the flaw of the Stokes mode expansion since we could compare with the correct and experimentally confirmed onset of the Taylor-Couette instability. In other situations, preferably in transition to turbulence due to shear profiles where no eigenvalues are crossing the imaginary axis (as e.g. in pipe flow) this comparison is not available. One should keep in mind the limited accuracy of Stokes mode expansions, nevertheless. The pipe flow results [5] might not be affected, since there are no moving walls. Investigating the direct transition to turbulence without explicit instability as it happens for rotating outer cylinder but nearly resting inner one in Taylor-Couette geometry, one better avoids a Stokes mode expansion [9].

Acknowledgements

This work was supported by the Deutsche Forschungsgemeinschaft via Sonderforschungsbereich 185 (Nichtlineare Dynamik).

[1] G. Taylor, Stability of a viscous liquid contained between two rotating cylinders. Phil. Trans. Roy. Soc. London A **223,** 289 (1923).
[2] S. Chandrasekhar, Hydrodynamic and Hydromagnetic Stability. Oxford University Press, 1961.
[3] P. Drazin and W. Reid, Hydrodynamic Stability. Cambridge University Press, London 1981.
[4] H. Kuhlmann, D. Roth, and M. Lücke, Taylor vortex flow under harmonic modulation of the driving force. Phys. Rev. A **39,** 745 (1989).
[5] L. Boberg and U. Brosa, Onset of turbulence in a pipe. Z. Naturforsch. **43a,** 697 (1988).
[6] F. Marqués, On boundary conditions for velocity potentials in confined flows: Application to Couette flow. Phys. Fluids A **2,** 729 (1990).
[7] C. Andereck, S. Liu, and H. Swinney, Flow regimes in a circular Couette system with independently rotating cylinders. J. Fluid Mech. **164,** 155 (1986).
[8] R. C. Di Prima and H. Swinney, Instabilities and transition in flow between concentric rotating cylinders. In: Hydrodynamic Instabilities and the Transition to Turbulence (H. Swinney and J. Gollub, eds.). Springer-Verlag, Berlin 1985.
[9] T. Gebhardt and S. Grossmann, The Taylor-Couette eigenvalue problem with independently rotating cylinders. Preprint, 1991.
[10] L. D. Landau and E. M. Lifschitz, Course of Theoretical Physics, vol. 6: Fluid Mechanics. Pergamon Press, Oxford 1987.